

Local-field effects in linear response properties within an Polarizable Frozen Density Embedding method

Aparna K. Harshan, Mark J. Bronson Jr., and Lasse Jensen*

*Department of Chemistry, The Pennsylvania State University, 104 Chemistry Building,
University Park, 16802, United States.*

E-mail: jensen@chem.psu.edu

Abstract

In this work, we present a polarizable frozen density embedding method for calculating polarizabilities of coupled subsystems. The method (FDE-pol) combines a frozen density embedding method with an explicit polarization model such that the expensive freeze/thaw cycles can be bypassed, and approximate non-additive kinetic potentials are avoided by enforcing external orthogonality (EO) between the subsystems. To describe the polarization of the frozen environment, we introduce a Hirshfeld-partition-based density-dependent method for calculating the atomic polarizabilities of atoms in molecules which alleviate the need to fit the atomic parameters to a specific system of interest or to a larger general set of molecules. We show that the Hirshfeld-partition-based method predicts molecular polarizabilities close to the basis set limit and thus a single basis set dependent scaling parameter can be introduced to improve the agreement against the reference polarizability data. To test the model we characterized the uncoupled and coupled response of small interacting molecular complexes. Here the coupled response properties include the perturbation of the frozen system due to the

external perturbation which is ignored in the uncoupled response. We show that FDE-pol can accurately reproduce both the exact uncoupled polarizability and once local fields are included also the coupled polarizabilities of the supermolecular systems. Using damped response theory we also demonstrate that the coupled frequency-dependent polarizability can be described by including local field effects. The results emphasize the necessity of including local-field effects for describing the response properties of coupled subsystems, as well as the importance of accurate atomic polarizability models.

1 Introduction

There is a significant interest in developing models for describing the response properties of molecules embedded within an environment such as a solvent, protein or a surface. In quantum embedding methods, the larger chemical system is subdivided into fragments which are then treated separately and offers versatility for evaluating the properties for a large range of systems.¹⁻⁴ The natural drawback of dividing a large system into smaller constituent fragments is the resultant inadequate description of the interactions between the individual fragments due to challenges involved in accurately partitioning the electron density into subsystems. This becomes particularly significant when performing spectroscopic simulations for strongly coupled systems. To overcome this hurdle, and to have an accurate electronic structural description of the subsystems which is pivotal for simulating optical properties, various types of exact embedding methods have been developed.⁴⁻⁹

A popular approach to doing embedding calculations is subsystem DFT,¹⁰⁻¹⁶ where the entire system is partitioned into subsystems and the electronic structure is determined separately at the DFT level. Within subsystem DFT, exact embedding approaches can be achieved either by reconstructing the embedding potential^{9,17-19} or enforcing external orthogonality using projection operators.²⁰⁻²⁴ A common subsystem approach is frozen density embedding (FDE)^{25,26} where the total energy is minimized with respect to changes in one subsystems' density while the density of the other sub-

systems is kept frozen. In FDE, the total electron density is calculated from the sum of fragment densities, where both embedded system and environment densities are iteratively solved using a freeze-and-thaw approach.^{25,26} This method is in principle exact, however, in practice it typically relies on an approximate non-additive kinetic potential which tends to fail for strongly overlapping fragment densities.^{27,28} However, the need for the non-additive kinetic potential can be avoided by enforcing orthogonality between the orbitals of the different subsystems.^{20–24} Furthermore, recent work has shown that the computationally expensive freeze/thaw (FT) cycles can be avoided by including a polarization term in the embedding operator.²⁹

Another common strategy is quantum mechanics and molecular mechanics (QM/MM) models where the embedding operator is approximated based on a classical Hamiltonian.^{30–40} These models have been particularly successful in molecular simulations of large systems,⁴¹ due to the lower computational cost of describing the coupling of the subsystems. The mutual polarization of the subsystems can be accounted for using polarization embedding potentials^{42–48} which are particularly important for the prediction of response properties.^{43,49,50} The embedding potential typically consists of atomic point charges or higher multipoles representing the charge distribution of the MM system and atomic polarizabilities used to describe the induction energy.^{2,51} The parameters needed for the embedding potential are typically derived from quantum mechanical calculations.⁵² The quality of the embedding potential largely determines the size of the QM system needed for generating accurate results.² Polarization embedding methods can also be combined with a repulsion term based on a Huzinaga based projection operator which averts the electron spill-out from quantum to classical region⁵³ important for response properties.^{46,53–55}

Subsystem methods have also been extended to describe excited state properties^{25,56,57} or general response properties.^{4,58} The FDE method has been extended to TDDFT regime and can be implemented to make it a computationally efficient choice for calculating the response properties of large embedded systems.^{59,60} Within FDE-TDDFT one can differentiate between two approaches; the uncoupled and the coupled approach.

The first approach only accounts for the response of the active system and the response of the environment is neglected and the second includes the coupling to the environment response. The uncoupled approach is suited for studying localized excitations but fails when describing excitations delocalized over different subsystems.^{4,25,56–58} The coupled TDDFT approach combined with the projection based embedding can exactly reproduce supermolecular DFT results for both delocalized excitations and other response properties such as polarizabilities.^{56,57} Within a polarizable QM/MM approach the response of the environment can be incorporated through the so-called local field effects which accounts for the polarization of the MM region by the external perturbation.^{46,47,61–65} The inclusion of the local field effects have been shown to have resulted in greater accuracy for oscillator strengths and two-photon absorption cross-sections calculated with the polarizable density embedding.⁵³ Local field effects are also essential for describing the interactions between molecules and plasmonic nanoparticles for example for describing surface-enhanced Raman spectroscopy (SERS).^{66–68}

In this work, we extend the polarizable frozen density embedding method²⁹ for describing response properties of molecules coupled to an environment. The method (FDE-pol) combines a frozen density embedding method with an explicit polarization model such that the expensive freeze/thaw (FT) cycles can be bypassed. Furthermore, the need for an approximate non-additive kinetic potential (NAKP) is circumvented by enforcing external orthogonality (EO) between the subsystems. Previously, the polarization of the environment used atomic polarizabilities obtained either by fitting to the specific system of interest or to a larger general set of molecules. In this work, we introduce a density-dependent method for calculating the atomic polarizabilities of atoms in molecules which alleviate the need for fitting the atomic parameters. We show that FDE-pol can accurately reproduce the exact uncoupled polarizability for a series of interacting molecular complexes. Furthermore, we show that the coupled polarizabilities of the supermolecular systems can be reproduced once local field effects are included. Comparison between different polarization models using uncoupled response showed little differences due to the small effects of the polarization. However, once

local field effects are included larger differences can be found showing that an accurate polarization model is necessary for reproducing the supermolecular response. Inclusion of local field effects with polarizable embedding models therefore offers a more stringent test of the model and should be considered when benchmarking.

2 Theory

In the FDE-pol method the density of the environment is kept frozen but mutual polarization is accounted for through a polarization operator.²⁹ We have previously shown that the inclusion of the polarization term enables to avoid computationally expensive freeze/thaw cycles while still providing accurate results for the active fragment. The use of the projection operator avoid the need for using an approximate non-additive kinetic energy term and thus enables strongly interacting densities to be considered.

2.1 The FDE-pol method

In the following we will denote the density of the active fragment as ρ_I and the density of the frozen environment by ρ_{II}^0 . In the FDE-pol method we can write the total energy as

$$\begin{aligned}
 E[\rho_I] = & T_s[\rho_I, \rho_{II}^0] + V_{nuc}[\rho_I, \rho_{II}^0] + J[\rho_I, \rho_{II}^0] + V_{nn} + E^{\text{XC}}[\rho_I, \rho_{II}^0] \\
 & + E^{\text{EO}}[\rho_I, \gamma_{II}^0] + E^{\text{ind}}[\rho_I, \delta\rho_{II}^0]
 \end{aligned}
 \tag{1}$$

where T_s is the non-interacting kinetic energy for which the non-additive kinetic energy is zero as the EO projection operator enforces orthogonality between the orbitals in system I and II, $V_{nuc}[\rho_I, \rho_{II}^0]$ is the electron-nuclei potential, $J[\rho_I, \rho_{II}^0]$ is the Coulombic electron-electron interaction term, V_{nn} represent the nucleus-nucleus repulsion. The total exchange-correlation functional is contained in $E^{\text{XC}}[\rho_I, \rho_{II}^0]$. $E^{\text{EO}}[\rho_I, \gamma_{II}^0]$ is the EO contribution that ensures the orbitals in I are orthogonal to II and the non-local

functional is given by

$$E^{\text{EO}}[\rho_I, \gamma_{II}^0] = \mu \int \rho_I(r) S^{I,II} \gamma_{II}^0(r, r') S^{II,I} dr dr' \quad (2)$$

where μ is a scaling parameter, μ ($\mu \sim 10^6 E_h$),²⁴ the frozen density matrix in system II is denoted by γ_{II}^0 and $S^{I,II}$ are the overlap matrices between the MOs of the two subsystems. The final term is the induction energy describing the many-body polarization energy^{69,70}

$$E^{\text{ind}}[\rho_I, \delta\rho_{II}^0] = -\frac{1}{2} \int V^{\text{SCF}}(r) \delta\rho_{II}^0(r) dr \quad (3)$$

where $\delta\rho_{II}^0(r)$ is the induced density in system II due to the potential, $V^{\text{SCF}}(r)$, arising from the charge distribution ρ_I in system I . Introducing the non-local polarizability $\alpha_{\beta\gamma}(r, r')$ we can write the induction as^{69,70}

$$E^{\text{ind}} = -\frac{1}{2} \int F_{\beta}^{\text{SCF}}(r) \alpha_{\beta\gamma}(r, r') F_{\gamma}^{\text{SCF}}(r') dr dr' \quad (4)$$

where F_{β}^{SCF} is the field along the β -direction.

The calculation of induction energy in this way would require solving the linear response equations for system II to generate the non-local polarizability. However, this becomes computationally too demanding. Therefore, we will coarse-grain the induction energy in terms of atomic dipolar contributions as

$$E^{\text{ind}} = -\frac{1}{2} \sum_{m,n} F_{\beta}(r_m) B_{mn,\beta\gamma} F_{\gamma}(r_n) \quad (5)$$

where we have approximated the non-local polarizability in terms of the classical dipole-dipole response matrix, $B_{mn,\beta\gamma}$. The classical response matrix, $\mathbf{B} = \mathbf{A}^{-1}$, can be obtained by solving the classical linear response equations

$$\mathbf{A}\mu^{\text{ind}} = \mathbf{F}^{\text{SCF}}, \quad (6)$$

where the matrix \mathbf{A} describes the dipole-dipole interactions including self-interactions

and is given by

$$A_{mn,\alpha\beta}(\omega) = \begin{cases} \alpha_{m,\alpha\beta}^{-1} & m = n, \\ -T_{mn,\alpha\beta} & m \neq n. \end{cases} \quad (7)$$

where $\alpha_{m,\alpha\beta} = \delta_{\alpha\beta}\alpha_m$ is the isotropic atomic polarizability and $T_{mn,\alpha\beta}$ is the screened dipole-dipole interaction tensor.⁷¹ The atomic polarizabilities are related to the polarizable volume as shown in the Supporting Information. Previously, we have used fixed atom-type polarizability parameters, whereas in reality the polarizable volume of an atom in a molecule is sensitive to the environment effects caused by the presence of neighboring atoms. Therefore, in this work we will adapt a density dependent polarizabilities given by⁷²

$$\alpha_m[\rho(\mathbf{r})] = \frac{\int r^3 w_m(\mathbf{r}) \rho(\mathbf{r}) d^3\mathbf{r}}{\int r^3 \rho_m^{\text{free}} d^3\mathbf{r}} = \frac{V_m^{\text{eff}}}{V_m^{\text{free}}} \alpha_m^{\text{free}} \quad (8)$$

where the effective volume of an atom in molecule is obtained from the Hirshfeld partitioning of total electron density with the following weights,

$$w_m(\mathbf{r}) = \frac{\rho_m^{\text{free}}(\mathbf{r})}{\sum_n \rho_n^{\text{free}}(\mathbf{r})} \quad (9)$$

The free atom polarizabilities are taken from Ref.⁷³ The Hirshfeld partitioning has previously been used to describe density-dependent dispersion coefficients.⁷⁴

The atomic dipoles are smeared out by a Gaussian charge distribution to avoid overpolarization which leads to the following form for the dipole-dipole interaction tensor^{71,75–78}

$$T_{ij,\alpha\beta}^{(2)} = \frac{3r_{ij,\alpha}r_{ij,\beta} - \delta_{\alpha\beta}r_{ij}^2}{r_{ij}^5} \left[\text{erf}\left(\frac{r_{ij}}{R_{\mu\mu}^{ij}}\right) - \frac{2}{\sqrt{\pi}} \frac{r_{ij}}{R_{\mu\mu}^{ij}} e^{-(r_{ij}/R_{\mu\mu}^{ij})^2} \right] - \frac{4}{\sqrt{\pi}(R_{\mu\mu}^{ij})^3} \frac{r_{ij,\alpha}r_{ij,\beta}}{r_{ij}^2} e^{-(r_{ij}/R_{\mu\mu}^{ij})^2} . \quad (10)$$

for the dipole-dipole interactions where $R_{\mu\mu}^{ij} = \sqrt{(R_{\mu}^i)^2 + (R_{\mu}^j)^2}$. The parameters R_{μ}^i are effective radii and can be uniquely defined in terms of the polarizability and by

taking the limit $r_{ij} \rightarrow 0$ as

$$R_\mu^i = \left(\sqrt{\frac{2}{\pi}} \frac{\alpha_i}{3} \right)^{1/3} \quad (11)$$

The KS equations are then obtained by minimizing the energy w.r.t the density which gives

$$\left[-\frac{1}{2} \nabla^2 + v_{\text{eff}}^{\text{KS}}[\rho_I] + v_{\text{eff}}^{\text{emb}}[\rho_I] \right] \phi_i^I = \epsilon_i \phi_i^I \quad (12)$$

where $v_{\text{eff}}^{\text{KS}}[\rho_I]$ is the standard KS effective potential,⁷⁹ ϵ_i are the orbital energies, and the embedding potential is given by

$$v_{\text{eff}}^{\text{emb}}[\rho_I] = v_{II}^{\text{nuc}} + \int \frac{\rho_{II}(r')}{|r - r'|} dr' + \frac{\delta E_{\text{XC}}^{\text{nadd}}[\rho_I, \rho_{II}^0]}{\delta \rho_I} + v^{\text{EO}}[\gamma_{II}^0] + v^{\text{DIM}}[\rho_I] \quad (13)$$

The first two terms of Eq. 13 describe the nuclear and electronic potential due to system II , and the third term non-additive (nadd) components of the exchange-correlation (v_{xc}) potential. The fourth term is the non-local EO potential that ensures that the KS orbitals of the subsystems mutually orthogonal and is given by

$$v^{\text{EO}}[\gamma_{II}^0] = \mu \sum_{r,s \in II} S_{pr}^{I,II} \gamma_{rs}^0 S_{st}^{II,I} \quad (14)$$

based on the projection operator method, where the orbital energies of a subsystem were raised by a scaling parameter, μ ($\mu \sim 10^6 E_h$).²⁴ The final term is the polarization operator and is given by

$$v^{\text{DIM}}[\rho_I] = \sum_m T_{jm,\beta}^{(1)} \mu_{m,\beta}^{\text{ind}} \quad (15)$$

where $\mu_{m,\beta}^{\text{ind}}$ are the induced dipoles obtained by solving the linear response equations (Eq. 6), and $T_{ij,\alpha}^{(1)}$ is a first-order interaction tensor given by:

$$T_{ij,\beta}^{(1)} = \frac{r_{ij,\beta}}{r_{ij}^3} \left[\text{erf} \left(\frac{r_{ij}}{a^{\text{scr}}} \right) - \frac{2}{\sqrt{\pi}} \frac{r_{ij}}{a^{\text{scr}}} e^{-\left(\frac{r_{ij}}{a^{\text{scr}}} \right)^2} \right] \quad (16)$$

where a^{scr} is a screening parameter used to avoid over-polarization. By default, a^{scr} is set to 1 a.u.

2.2 Response theory within the FDE-pol method

To derive the response equations within the FDE-pol method, we will follow the quasi-energy formulation of response theory^{80,81} The quasi-energy formalism enables frequency dependent molecular response properties to be obtained as energy derivatives similar to ground state properties.^{80,81} Furthermore, the quasi-energy formalism ensures that the molecular response functions retain the correct symmetry properties with respect to interchanging of response operators.^{80,81} Finally, the quasi-energy formalism becomes important when deriving molecular properties that includes local field effects.⁴⁷ As we will show in the following, the inclusion of local field effects are necessary for direct comparison with super-molecular simulations. The damped response functions will then be obtained by incorporating a complex orbital energy ($\varepsilon_i - i\Gamma$) where Γ corresponds to an energy broadening term that can be related to the finite lifetime of the excited state.⁸²⁻⁸⁴ We can write the the quasi-energy as

$$Q(t) = E(t) - i \sum_i \langle \phi_i | \frac{\partial}{\partial t} | \phi_i \rangle \quad (17)$$

where ϕ_i are the time-dependent KS orbitals, and the time-dependent energy is given by

$$E(t) = \sum_{\mu\nu} D_{\mu\nu}(t) \langle \chi_\mu | h(t) | \chi_\nu \rangle + \frac{1}{2} \sum_{\mu\nu} D_{\mu\nu}(t) \langle \chi_\mu | V_c[\rho(t)] | \chi_\nu \rangle \quad (18)$$

$$+ E^{\text{XC}}[\rho(t)] + E^{\text{EO}}[\rho(t)] + E^{\text{ind}}[\rho(t)]$$

Here $\rho(t)$ is the perturbed density for system I, $D_{\mu\nu}(t)$ is the corresponding density matrix, and $V_c[\rho(t)]$ is the Coulomb potential. χ_μ are the basis functions, which are assumed to be independent of the perturbation. This is fine for the electric field perturbations consider here, however, for magnetic perturbation one also has to consider the additional time-dependence of the basis sets.⁸⁵ The one-electron operator $h(t)$ contains

the time-dependent electric field perturbation and is given by

$$h(t) = h^0 + V_\beta^{\text{ext}} = h^0 + \varepsilon^\beta (e^{\pm i\omega t} + 1) \cdot \hat{\mu}_\beta \quad (19)$$

where ε is the field strength and β indicates the direction of the electric field perturbation. We can then expand the density matrix in terms of the perturbation as

$$D = D^0 + [e^{\pm i\omega t} D^\beta(\pm\omega) + D^\beta(0)]\varepsilon^\beta + \dots \quad (20)$$

where the number of superscripts indicates the *order* of the perturbation.^{86,87} Molecular properties can then be obtained as the derivatives of the time-averaged quasi-energy

$$\{Q(t)\}_T = \frac{1}{T} \int_{-T/2}^{T/2} Q(t) dt \quad (21)$$

where $T = 2\pi/\omega_0$ is the period of the perturbation. For example, the frequency-dependent polarizability is given by

$$\alpha_{\beta\gamma}(-\omega, \omega) = - \left. \frac{d^2\{Q\}_T}{d\varepsilon_\beta d\varepsilon_\gamma} \right|_{\varepsilon=0} = - \sum_{\mu\nu} H_{\mu\nu}^\beta D_{\mu\nu}^\gamma(\omega) - \left. \frac{d^2\{E^{\text{ind}}\}_T}{d\varepsilon_\beta d\varepsilon_\gamma} \right|_{\varepsilon=0} \quad (22)$$

where the first term is the polarizability of perturbed subsystem *I* and the last term is the result of the interaction between subsystem *II* and the external perturbation. The term is given by

$$- \frac{d^2\{E^{\text{ind}}\}_T}{d\varepsilon_\beta d\varepsilon_\gamma} = - \frac{d}{d\varepsilon_\beta d\varepsilon_\gamma} \left[-\frac{1}{2} \sum_{mn} F_\beta^{\text{tot}}(r_m) B_{mn,\beta\gamma} F_\gamma^{\text{tot}}(r_n) \right] \quad (23)$$

$$= - \sum_{\mu\nu} \langle \chi_\mu | V_\beta^{\text{loc}}(\omega) | \chi_\nu \rangle D_{\mu\nu}^\gamma + \alpha_{\beta\gamma}^{II}(-\omega, \omega) \quad (24)$$

where $\alpha_{\beta\gamma}^{II}(-\omega, \omega)$ is the polarizability of the unperturbed system *II*, and the total electric field is given by

$$F_\beta^{\text{tot}}(r_m) = - \sum_{\mu\nu} D_{\mu\nu} \langle \chi_\mu | T_{mj,\beta}^{(1)} | \chi_\nu \rangle + F_\beta^{\text{nuc}} + \varepsilon^\beta e^{\pm i\omega t} \quad (25)$$

and contains the external electric field, ε^β . The local field operator is given by

$$V_\beta^{\text{loc}}(\omega) = \sum_{m,n} T_{mj,\beta}^{(1)} B_{mn,\beta\gamma} F_\gamma^{\text{unit}}(r_n) = \sum_m \mu_{m,\beta}^{\text{ind,ext}} T_{mj,\beta}^{(1)} \quad (26)$$

where $\mu_{m,\beta}^{\text{ind,ext}}$ is the induced dipoles due to a unit field $F_\gamma^{\text{unit}}(r_n)$. Therefore, we can write the total polarizability as

$$\alpha_{\beta\gamma}(-\omega, \omega) = - \sum_{\mu\nu} H_{\mu\nu}^\beta D_{\mu\nu}^\gamma(\omega) - \sum_{\mu\nu} \langle \chi_\mu | V_\beta^{\text{loc}}(\omega) | \chi_\nu \rangle D_{\mu\nu}^\gamma(\omega) + \alpha_{\beta\gamma}^{II}(-\omega, \omega) \quad (27)$$

The interactions between the external field and subsystem *II* thus give rise to two contributions. The second term is the local field contribution to the response. The local field response is due to the induced polarization in the subsystem *II* caused by the external electric field. The third term is simply the polarizability of the isolated subsystem *II* calculated using the classical response equations.

The first-order density matrix can be calculated using damped response theory.⁸⁸ As mentioned above the damped response equations cannot be derived directly using the quasi-energy approach but rather the damping term is added phenomenologically, the first-order density matrix is then given by

$$D^\beta(\pm\omega) = C^\beta(\pm\omega)nC^{0\dagger} + C^0nC^{\beta\dagger}(\mp\omega) \quad (28)$$

where n is the occupation number and $C^\beta(\mp\omega)$ are the first-order perturbed MO coefficients. The first-order perturbed MO coefficients are related to the unperturbed MO coefficients as $C^\beta(\pm\omega) = C^0U^\beta(\pm\omega)$ where $U^\beta(\pm\omega)$ is the first-order transformation matrix, given by

$$U_{ia}^\beta(\pm\omega) = \frac{G_{ia}^\beta(\pm\omega)}{\xi_a^0 - \xi_i^0 \mp \omega \mp i\Gamma} \quad (29)$$

where ξ_i and ξ_a are the one-electron energies for occupied and virtual orbitals respec-

tively, and G is the first-order KS matrix in the MO basis⁸⁶ given by

$$G_{ia}^{\beta}(\pm\omega) = \langle i | V_{\beta}^{\text{ext}} + V_{\beta}^{\text{loc}}(\omega) + V^{\text{Coul}}[\delta\rho_I] + V^{\text{XC}}[\delta\rho_I] + V_{\beta}^{\text{DIM}}[\delta\rho_I] | a \rangle \quad (30)$$

and we have introduced the Coulomb potential, $V^{\text{Coul}}[\delta\rho_I]$, exchange potential, $V^{\text{XC}}[\delta\rho_I]$, and DIM potential, $V_{\beta}^{\text{DIM}}[\delta\rho_I]$ due to the first-order perturbed density of system I . Note that the total polarizability in Eq. 27 depends on the local field both through the induced density and the additional term arising from the quasi-energy derivative of the induction energy. This ensures that the polarizability tensor is symmetric.

2.3 Computational Details

All computations were performed using a local version Amsterdam Density Functional 2019.⁸⁹ The geometries and reference polarizability components used for the molecular polarizability calculations presented here are taken from the QM7b data-set.⁹⁰ The polarizabilities were then calculated using the dipole interaction model⁷⁸ by substituting effective atomic polarizabilities from Hirshfeld method for the static atomic polarizabilities. The electron densities required for this were calculated with different combinations of functional and basis sets as mentioned in the corresponding plots. These polarizabilities are compared against the molecular polarizabilities from response calculations⁹¹ in ADF at the same level of DFT. To this end, two test systems are chosen, the 2-Aminopyridine with methanol (AP-MeOH) and 7-Hydroxyquinoline with water (HQ-H₂O). These systems were previously shown to give accurate excitation energies with frozen density embedding method.⁹² In this work we choose to analyze the polarizability because of its extreme sensitivity to the variations in electron density. For each supermolecule, the constituent fragments are pulled apart by displacing the solvent molecule along the Z -axis and then the polarizabilities are calculated at each point along the displacement using the Perdew-Wang functional (PW91)^{93,94} with TZP basis set from the ADF library unless otherwise stated. The polarizabilities were calculated at each point along the potential energy surface (PES) using FDE-pol(X), uEO-FT,

cEO-FT and full DFT (PW91/TZP). In FDE-pol(X) the X denotes the different atomic polarization models using in the calculations with X=H representing Hirshfeld atomic polarizabilities from Eq. 8, X=G represents the atomic polarizabilities fit to the CCSD results for the QM7b database,⁹⁰ and for X=D the atomic polarizabilities are obtained by fitting to the DFT polarizabilities for each specific molecule. The uEO-FT model corresponds to the exact uncoupled response and cEO-FT represents the exact coupled response which in this work is calculated using the finite difference method. The cEO-FT results exactly reproduce the supermolecular response when summed over all subsystems. In all the FDE calculations the scaling parameter, μ was kept as $10^6 E_h$ and the supermolecular basis set was used. Frequency-dependent polarizabilities were calculated using the adiabatic local density approximation (ALDA) kernel within the AOResponse module of ADF, for life-time $\Gamma = 0.01$ a.u.

3 Results and Discussion

3.1 Polarizability of free molecules

To test the accuracy of the density-dependent Hirshfeld method of calculating molecular polarizabilities we compare the results against the molecular polarizability components from the first 240 molecules of the QM7b data-set obtained using CCSD.⁹⁰ Previous work have shown that the density-dependent Hirshfeld method can reproduce the isotropic polarizability to around 12%.^{72,74} Figure 1 shows the isotropic molecular polarizability for molecules in the chosen data subset as calculated from DFT with different basis sets and the LDA functional compared with the polarizabilities from the Hirshfeld method for the same molecules. We find that the isotropic polarizabilities from Hirshfeld method showed an average percentage error of 28% to 11% (before scaling) where the error decreased with increasing basis set size. The polarizability predicted by the Hirshfeld method are found (see Figure S1) to be nearly independent of the basis set whereas the DFT results showed a significant basis set dependence with

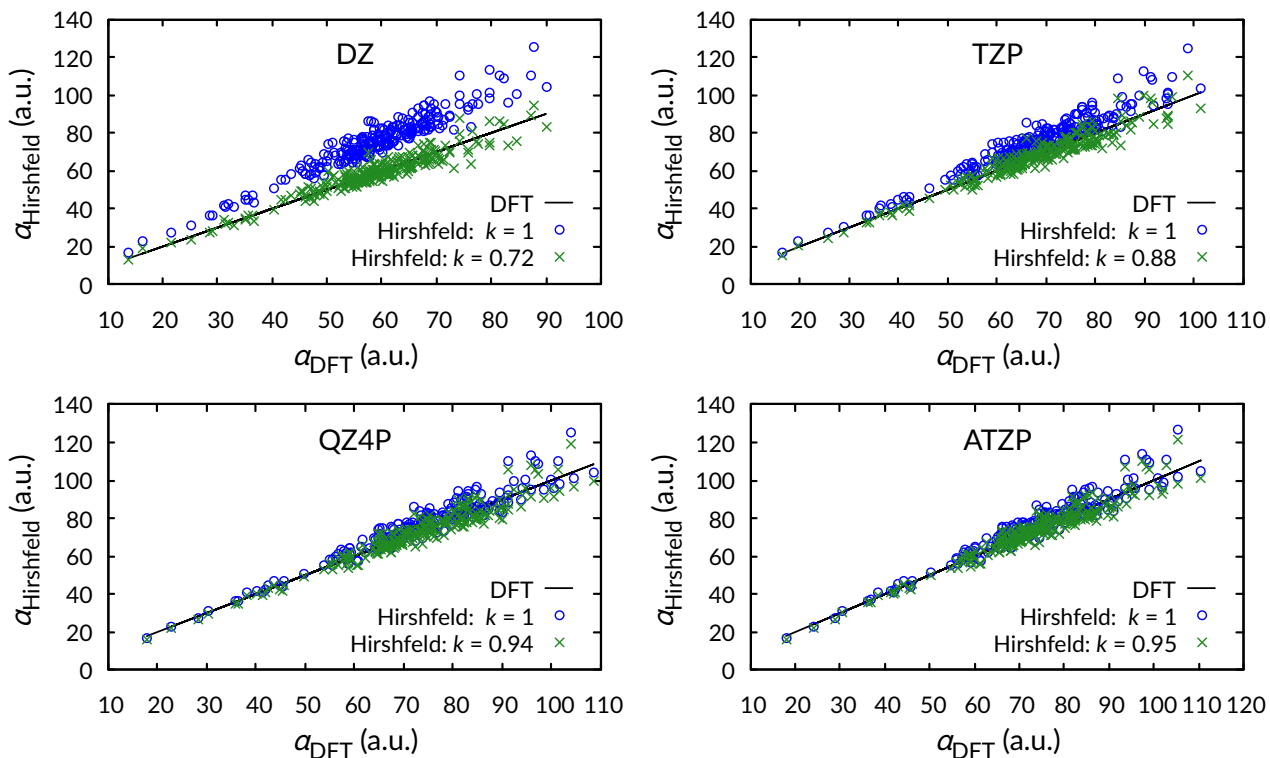


Figure 1: Isotropic polarizability from Hirshfeld vs DFT for different basis sets: scaled to get optimum fit.

the smaller basis sets predicting smaller polarizabilities as compared to the largest basis set. Hirshfeld partitioning is known not to be very sensitive to the size of the basis set and therefore likely predict atomic polarizabilities that are close to the basis set limit. This is consistent with the finding that the smallest mean deviation was found for the largest basis set and that the polarizability from the Hirshfeld method is systematically overestimated. Therefore, we chose to introduce a basis-set specific coefficient k that reduces the atomic polarizabilities so that the polarizabilities obtained from the Hirshfeld method match the DFT results. The polarizabilities calculated using the the scaling factor for the different basis sets are shown in Figure 1. With this basis set dependent scaling factor we find that the average percent errors for all basis sets were less than 10%. Since the scaling parameter has been determined from the isotropic polarizability we also show (see Figure S2) in the Supporting Information that the individual components show similar accuracy. The scaling parameter is also found to be independent

of the functional used as shown in Figure S3 in the Supporting Information and therefore reflects the differences in the basis sets. Alternatively, the atomic polarizability parameters can be fit directly to the QM7b data-set. The result of this fitting is shown in Figure S4 in the Supporting Information for the individual components. We find that this parameterization gives an average percentage error of 9% for the small subset and 5% for the complete set, and thus is comparable with the Hirshfeld method. The main advantages of the Hirshfeld method is that no parameterization is needed for new elements.

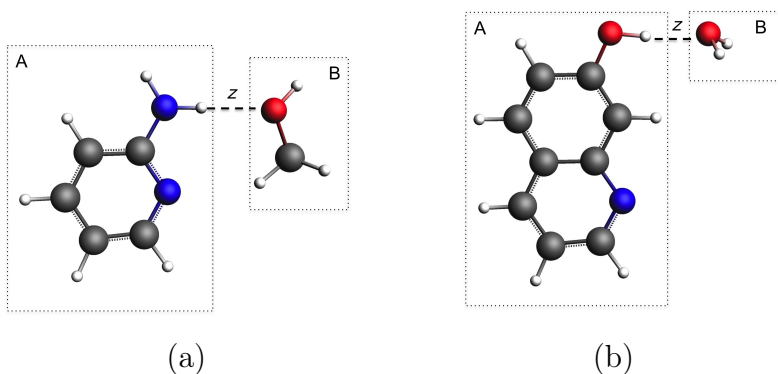


Figure 2: a) 2-Aminopyridine...MeOH and b) 7-Hydroxyquinoline...H₂O showing fragments A and B in each supermolecule. The inter-fragment distance is denoted by z .

Below we will benchmark the different FDE methods for complexes consisting of 2-Aminopyridine (AP) interacting with methanol (MeOH), and 7-Hydroxyquinoline (HQ) interacting with H₂O. The supermolecular systems and the displacement variables are shown in Figure 2. The dotted rectangles show the constituent fragments in each supermolecular system. For each system, the smaller molecule (MeOH or H₂O) was displaced along the Z-axis with the inter-fragment bond aligned with the same axis to calculate the electronic and response properties of the supermolecule as a function of the displacement variable.

We will compare three different parameterizations for the polarization model; (1) molecule specific parameters (DIM) obtained by fitting directly to the DFT results, (2) general parameters obtained by fitting to the QM7b set of molecules, and (3) Hirsh-

Table 1: Polarizability components for each fragment molecules from DFT and DIM, Global, and Hirshfeld parameters. All numbers are in atomic units (bohr³)

	DFT	DIM	Hirshfeld	Global
	α_{xx}			
AP	96.36	95.88	103.97	95.66
MeOH	22.47	22.41	23.77	30.95
HQ	165.67	169.62	146.57	132.62
H ₂ O	8.40	8.45	7.55	9.33
	α_{yy}			
AP	44.71	45.06	38.28	35.80
MeOH	19.22	19.22	18.35	26.23
HQ	72.54	72.30	59.56	56.81
H ₂ O	9.19	9.15	11.27	14.32
	α_{zz}			
AP	80.72	81.71	86.89	77.71
MeOH	19.57	19.52	18.86	26.75
HQ	122.77	122.96	119.74	115.45
H ₂ O	8.17	8.25	6.73	8.29

feld effective atomic polarizabilities. The DIM parameters were fit so as to give <3% error with respect to the DFT polarizabilities for each molecules. Table 1 shows the polarizability components for each fragment molecule as calculated from the specific fit (DIM), Hirshfeld, general fit (global), and full DFT methods. The atomic polarizability parameters are shown in Table S2 of the Supporting Information. Interestingly, we find that the Hirshfeld gives parameters which are similar across the different molecules and to that obtained from the general fit. In contrast, the atomic parameters from the specific fit are very different for each molecule. This is expected since in the specific fit the atomic parameters can be chosen to reproduce both the isotropic and anisotropic part of the polarizability and likely there are more than one set of parameters that offers similar accuracy in describing the polarizability. The percentage errors of polarizability components for each molecule as obtained from these three methods are given in Table S1. Based on that data, the percentage error for isotropic polarizability with reference to the corresponding DFT data varied from 3% to 22% for Hirshfeld method, whereas the general parameter fit had an error in the range of 1% to 55%. In general, the Hirshfeld and general parameters give polarizabilities of similar accuracy.

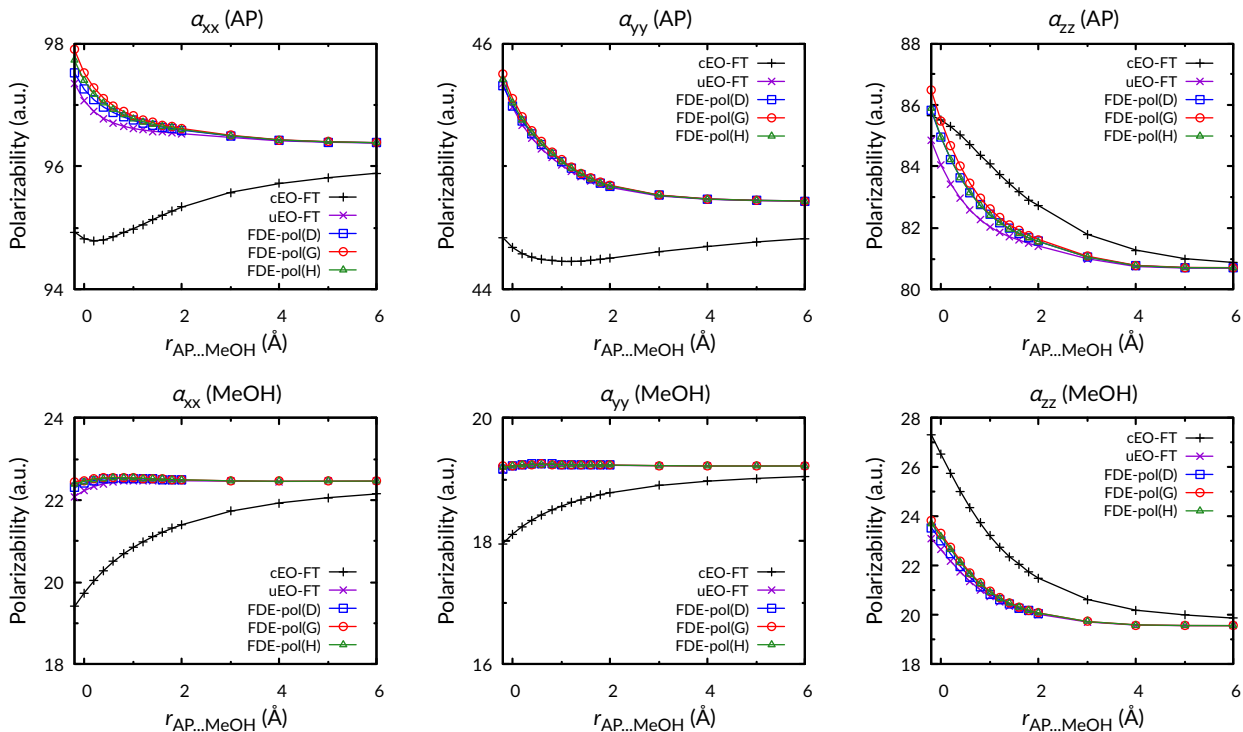


Figure 3: Fragment-wise individual polarizability components against inter-fragment distance for 2-Aminopyridine...MeOH using different methods, without local field (uncoupled response). Top: 2-aminopyridine as the active fragment, bottom: MeOH as the active fragment.

3.2 Uncoupled Polarizability of supermolecules from FDE-pol

To benchmark the FDE-pol calculations of the uncoupled polarizabilities we will compare against the uEO-FT results which represent the exact uncoupled polarizabilities for the given functional and basis set. Figure 3 shows the fragment-wise individual polarizability components against inter-fragment distance for AP–MeOH using different methods, and Figure 4 shows that for the (HQ–H₂O) system. In Figure 3, the top row are the polarizability components for the AP molecule with AP as the active system and MeOH kept frozen, whereas the bottom row shows the polarizability components for MeOH, with the active and frozen fragments switched, that is MeOH as the active fragment and AP as the frozen fragment. Similarly in Figure 4, the top row contains polarizability components for HQ molecule with HQ as the active system and H₂O kept

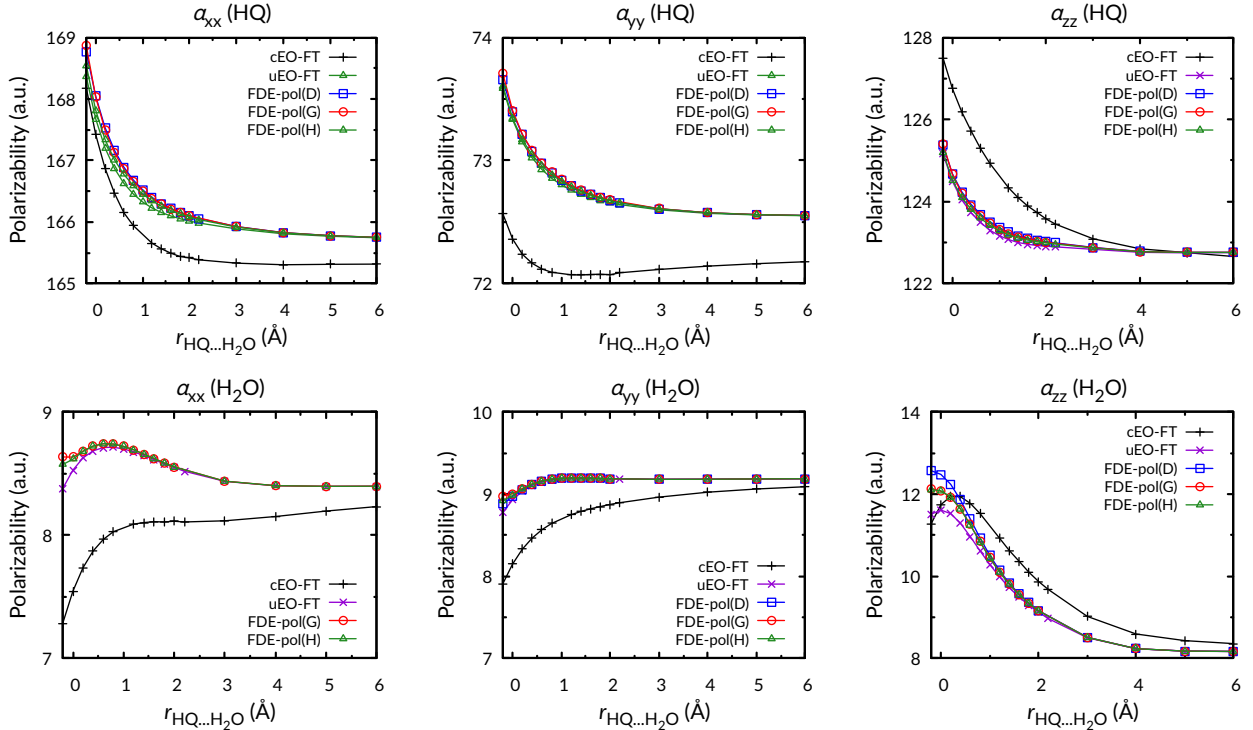


Figure 4: Fragment-wise individual polarizability components against inter-fragment distance for 7-Hydroxyquinoline...H₂O using different methods, without local field (uncoupled response). Top: 7-Hydroxyquinoline as active fragment, bottom: H₂O as active fragment.

frozen, and bottom row contains the polarizability components for H₂O molecules with HQ as the frozen fragment.

We see that for the larger fragments (AP and HQ) the polarizability components increase as the separation decreases with the largest increases for the component (ZZ) along the separation axis. For the two smaller fragments (MeOH and H₂O) we find smaller changes for the XX and YY components and again an increase in the ZZ polarizability component as the distance is decreased. In general, we find that the FDE-pol results agree well with the uEO-FT results independently of the polarization model used, with an error percentage less than 10% for all polarizability components. The largest error amongst these was for the ZZ component of the H₂O fragment, with a percent error of 9.2%. At the shortest separations FDE-pol tends to slightly overestimate the polarizabilities which could indicate a small over-polarization. However, small changes to the short-range screening (a^{scr}) of the polarization operator did not lead to

significantly better agreement and was not considered further.

In each of these plots, we also plot the coupled polarizabilities obtained using cEO-FT. The sum of the coupled polarizabilities exactly reproduces the supermolecular DFT results. Comparing the coupled polarizabilities with the uncoupled polarizabilities we see that they are significantly lower for the XX and YY components and larger for the ZZ components. The coupled polarizabilities include the response of both systems to the external perturbation whereas the uncoupled polarizability neglects the response of the frozen system to the external perturbation. Therefore, the response from the frozen fragment screens the external electric field in the XX and YY directions but enhances it along the ZZ direction. This leads to a significant change to the anisotropic polarizability whereas the isotropic polarizability is much less affected. Therefore, it is important to look at all the diagonal components of the polarizability tensor and not only the isotropic polarizability when analyzing the perturbation due to the surrounding environment.

3.3 Coupled Polarizability of supermolecules from FDE-pol

To describe the coupled polarizability we need to consider the response of the frozen system to the external perturbation. Within FDE-pol method this is done by including local field effects when calculating the polarizability. Once the local field effects are included in the FDE-pol simulation the obtained polarizability will contain the changes to the polarizability of both fragments as shown in Eq. 24. Therefore, to compare with the supermolecular calculation we will consider an effective polarizability of the active fragment defined as

$$\alpha_{\beta\beta}^{\text{active}} = \alpha_{\beta\beta}^{\text{supermolecule}} - \alpha_{\beta\beta}^{\text{frozen}} \quad (31)$$

where β is x, y , or z . In this way the polarizability of the active fragment includes changes to the polarizability of the frozen system and thus is consistent with the polarizability obtained in FDE-pol. The active fragment polarizabilities for the AP-MeOH

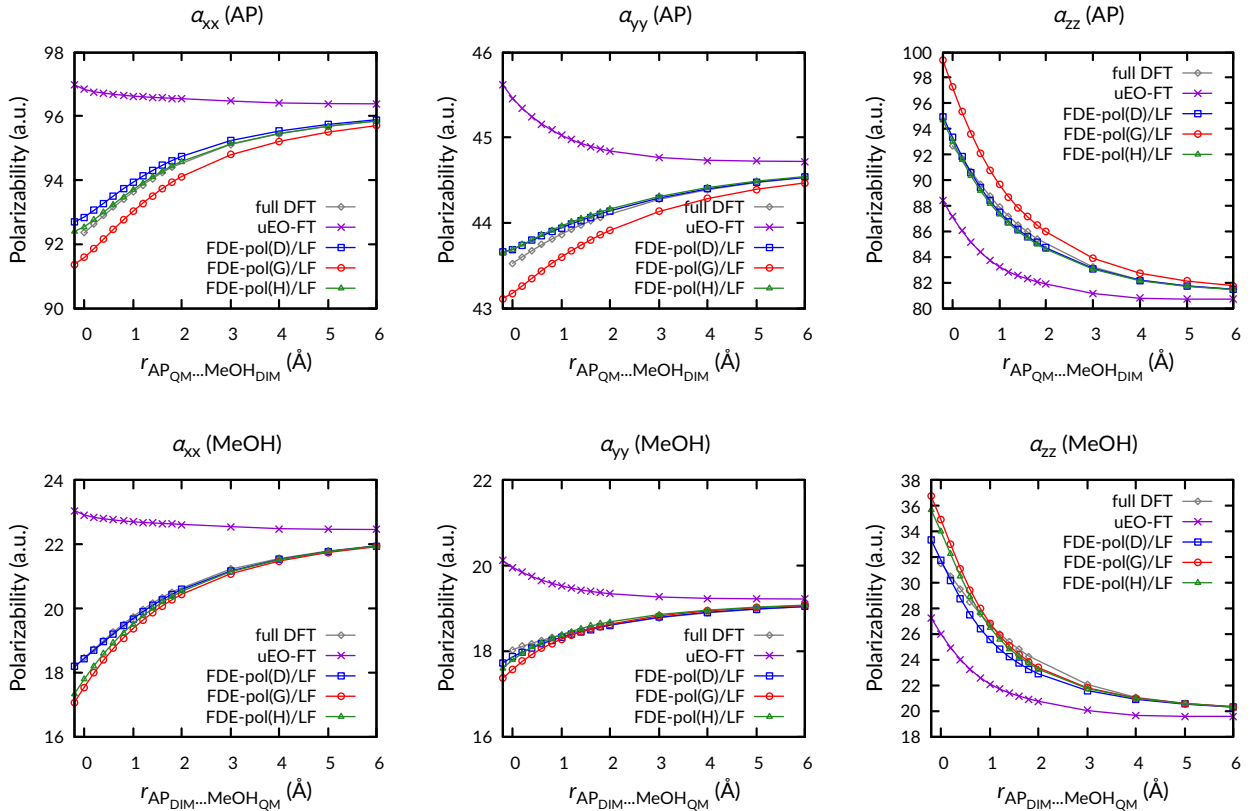


Figure 5: Effective polarizability components vs the inter-fragment distance for the 2-Aminopyridine...MeOH system including local field effects (coupled response). Top: 2-aminopyridine as the active fragment, bottom: MeOH as the active fragment.

system are shown in Figure 5 where the top row are the polarizability components for the AP molecule as the active system, whereas the bottom row shows the polarizability components for MeOH as the active and frozen fragments. Similarly in Figure 6, the top row contains polarizability components for HQ as the active system, and bottom row contains the polarizability components for H₂O molecules as the active fragment. For comparison we have also included the uncoupled polarizability calculated using uEO-FT which does not include the response of the frozen system to the external field.

For the AP–MeOH system shown in Figure 5 we see that the FDE-pol model accurately reproduces the effective polarizability of the active fragment. The largest deviations is found for FDE-pol(G) parameterization especially for the AP active fragment. This reflects that the global parameterization of the polarizability of MeOH

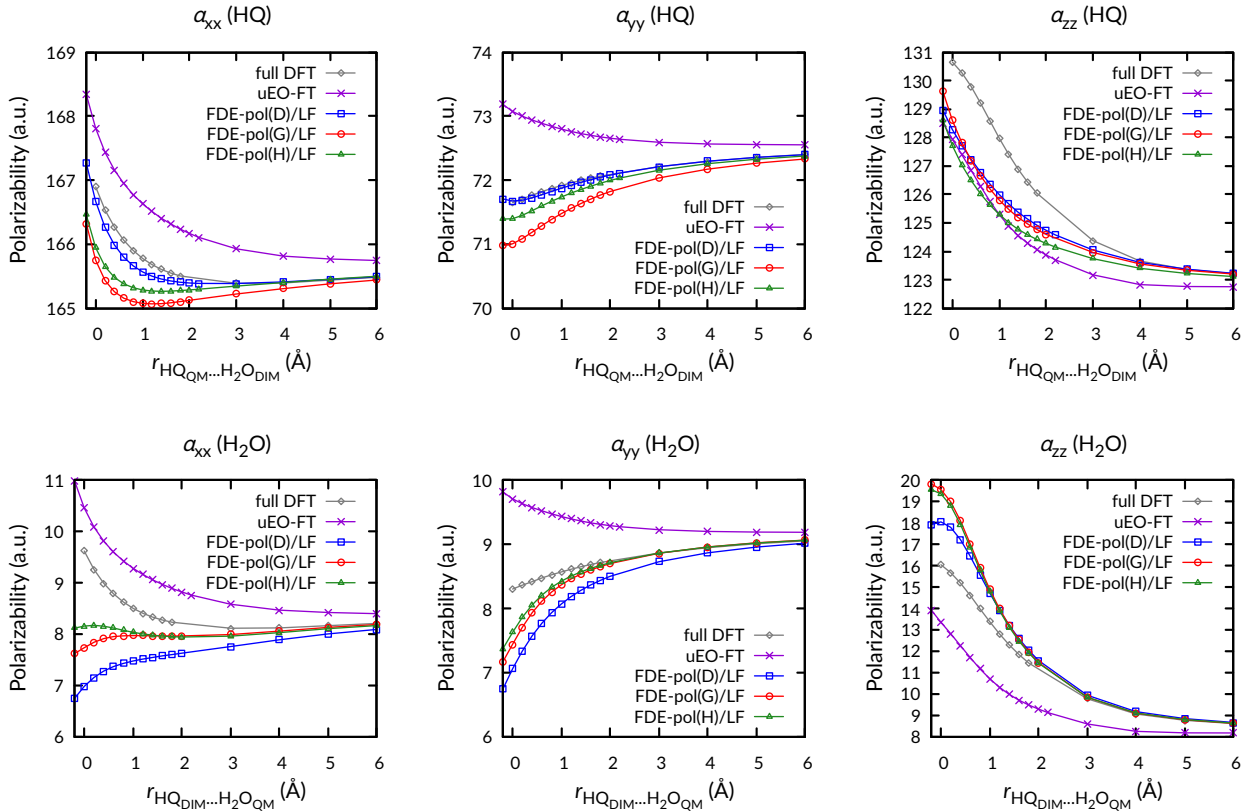


Figure 6: Effective polarizability components vs the inter-fragment distance for the 7-Hydroxyquinoline...H₂O system including local field effects (coupled response). Top: 7-hydroxyquinoline as the active fragment, bottom: H₂O as the active fragment.

shows the largest errors and therefore does not predict the local fields accurately. This is in contrast to the uncoupled polarizabilities where the different parameterization of FDE-pol(X) lead to very similar results. Once local field is included the accuracy of the classical polarization model becomes more important and serves as a more stringent test of the parameterization. Comparison with the uncoupled results in Figure 5 shows that the screening of the external field in the XX and YY direction and enhancement along the ZZ direction is captured correctly by the local field effects.

For the effective polarizabilities for HQ shown in Figure 6 we see that the best description is obtained using the FDE-pol(D) parameterization which is consistent with the accuracy of the DIM parameterization for H₂O. Surprisingly, for H₂O the FDE-pol(D) parameterization gives the worst agreement even though the polarizability of

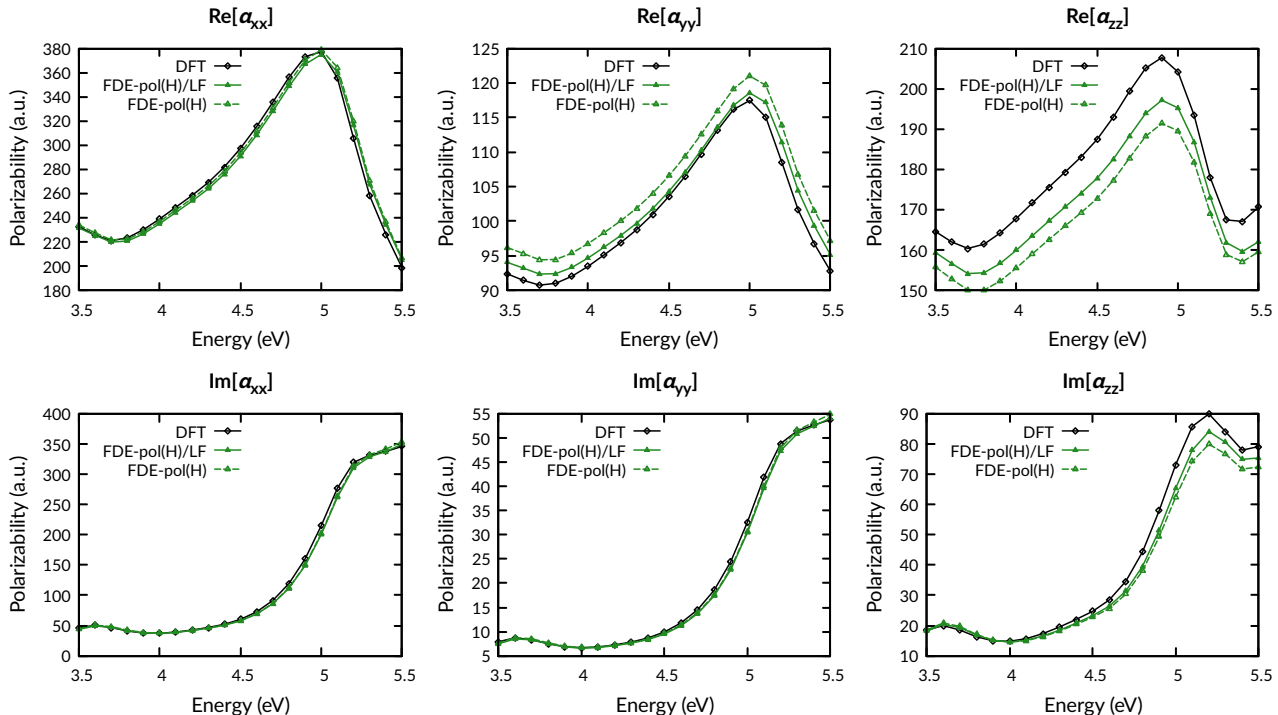


Figure 7: Frequency dependent polarizability components (diagonal) for the 7-Hydroxyquinoline...H₂O system at equilibrium geometry. FDE-pol(H) calculations with HQ as the active fragment and H₂O as frozen fragment is compared to supermolecular calculations using full DFT methods. ‘LF’ indicates that local field effects (coupled response) were included in the calculation.

the frozen system (here HQ) is accurately reproduced by the parameterization. In general, the FDE-pol(X) method struggles to accurately describe the effective polarizability of H₂O. However, this is likely a result of how well FDE-pol(X) described the uncoupled polarizability which already indicated an over polarization as described above. For all other systems the FDE-pol(D) parameterization provides the best agreement with supermolecular result due to the improved description of the polarizability of the frozen system. We also see that FDE-pol(H) tends to perform similarly or better than the FDE-pol(G) parameterization which again shows that obtaining the polarizability parameters from the atomic Hirshfeld volumes is an alternative to obtaining general atom type parameters by fitting to a large data set.

3.4 Frequency-dependent polarizabilities from FDE-pol

Local field effects are also expected to be important when considering the frequency-dependent polarizability. To test this we calculated the real and imaginary part of the polarizability of the HQ-H₂O system between 3.5-5.5 eV. These results were obtained at the equilibrium geometry ($r = 0$) and using HQ as the active fragment and water as the frozen fragment. The energy range was chosen on the basis of the excitation energies of the supermolecule, for which the lowest excitation energy was calculated to be at 3.6 eV and a strong transition at 5.2 eV at this level of theory (PW91/TZP). This strong excitation is localized on the HQ fragment and therefore should be captured by FDE-pol(H). In Figure 7 we plot the real and imaginary polarizability of HQ-H₂O calculated using the FDE-pol(H) method. Both the uncoupled (without local field) and coupled (with local fields) response are compared with the supermolecule DFT results. Here we consider the diagonal elements of the polarizability tensor and the corresponding data for the off-diagonal components are shown the Supporting Information in Figure S6. The frequency dependent polarizability is characterized by a large increase in the real polarizability around 5 eV and a corresponding increase in the imaginary polarizability around 5.2 eV due to the strong excitation localized in the HQ fragment at 5.2 eV. In general we find good agreement between the FDE-pol(H) results and the supermolecular DFT results and that the agreement is improved upon the inclusion of local field effects in the calculations. In particular, we find that the local field increases the ZZ-component and decreases the YY component. The XX-component is largely unaffected by the inclusion of local field effects. The largest deviations are found for the ZZ-components but that reflects the slight underestimation of the static polarizability using the FDE-pol(H) model. We find that the local field effect is the largest for the real part of the polarizability and only significant for the imaginary polarizability along the ZZ components around 5.2 eV. Since the water molecule is aligned with the Z-direction the strongest influence of the local field should be along this direction. The larger contribution of the local fields to the real part of the polarizability can be rationalized by considering the number of excited states contributing to the polarizability. Near

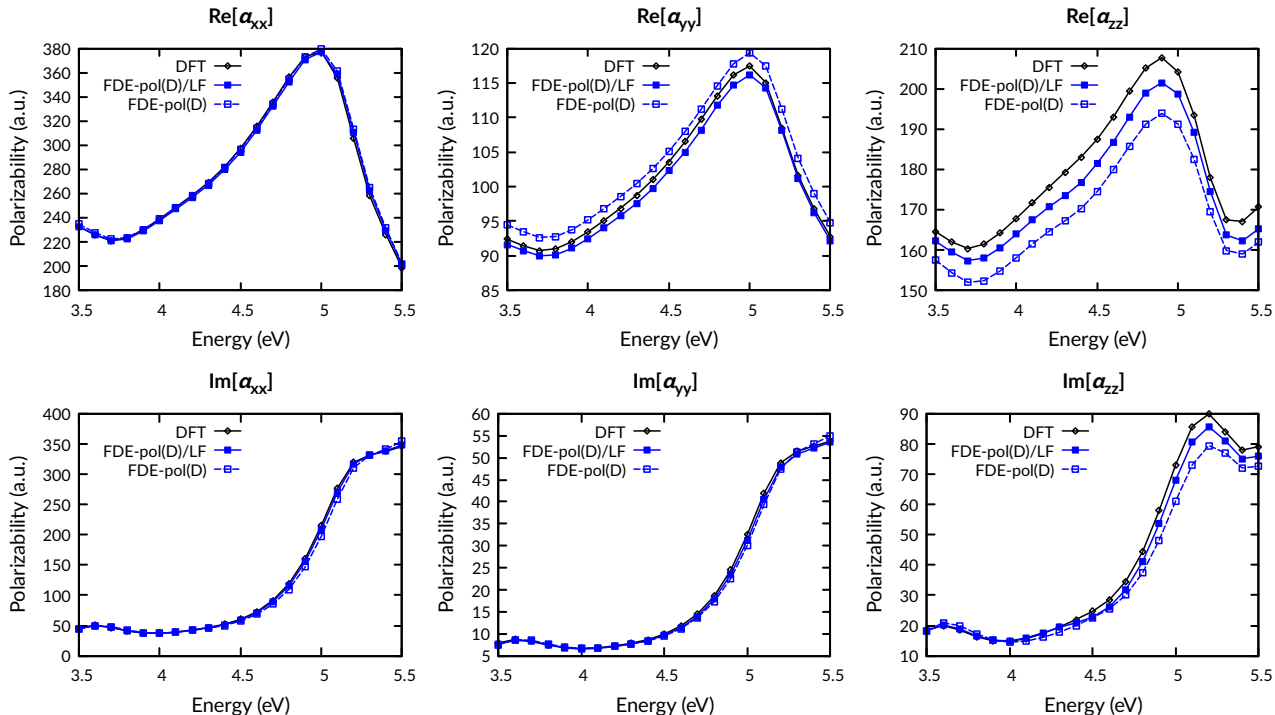


Figure 8: Frequency dependent polarizability components (diagonal) for the 7-Hydroxyquinoline...H₂O system at equilibrium geometry. FDE-pol(D) calculations with HQ as the active fragment and H₂O as frozen fragment is compared to supermolecular calculations using full DFT methods. ‘LF’ indicates that local field effects (coupled response) were included in the calculation.

a resonance the imaginary polarizability is dominated by that particular excited state whereas the real part has contribution from several electronic states. Since the local field couples into all these states the contribution to the real part of the polarizability can be expected to be larger.

Since the frequency-dependency of the polarizability obtained using FDE-pol(H) is very similar to that of the supermolecular results it indicate that the main differences is in the description of the static polarizability. The Hirshfeld parameterization significantly underestimates the ZZ component of the polarizability of water which likely results in the larger deviations for the coupled and uncoupled response in this direction. To verify this we calculated the frequency-dependent polarizability using FDE-pol(D) where the polarization model is molecule-specific. In Figure 8 we plot the coupled and uncoupled real and imaginary polarizability of HQ-H₂O calculated using

the FDE-pol(D) method. This shows that the polarizabilities from the molecule-specific fit (FDE-pol(D)) is in better agreement than the density dependent Hirshfeld (FDE-pol(H)), but both methods give smaller than 5% mean average error with respect to DFT. Off-diagonal elements have larger mean deviation than diagonal elements but within 18% when not including local field and 12% when local field is included (see the Supporting Information). We note that the ZZ component is improved due to the better description of the polarizability of the water fragment using the molecule specific parameterization. Thus, the inclusion of local field effects significantly improves the agreement with the supermolecular results in particular for the real part of the polarizability. In all of these calculations the frequency dependent response of the frozen-fragment has been ignored. However, the dispersion in the polarizability of water is small as long as it is not near an electronic resonance and therefore likely negligible. If the incident frequency is near an electronic resonance in the frozen-fragment the frequency-dependent response cannot be ignored.

4 Conclusions

We have presented a polarizable frozen density embedding (FDE-pol) method for calculating polarizabilities of coupled subsystems. A frozen density embedding is combined with an explicit polarization model and external orthogonality (EO) between the subsystems is enforced. The polarization model is based on a Hirshfeld-partition-based density-dependent method for calculating the atomic polarizabilities of atoms in molecules. This enables both the induction energy and the response of the frozen environment to be described without the need for fitting of atom type parameters. We found that the Hirshfeld-partition-based method predicts molecular polarizabilities close to the basis set limit. The introduction of a basis set dependent scaling parameter was shown to improve the agreement with the reference data. In general, we found that the Hirshfeld-partition-based method works as well as as a polarization model obtaining by fitting atom-type parameters to a large data base of molecular polarizabilities. To test

the model we characterized the uncoupled and coupled response of complexes consisting of 2-Aminopyridine (AP) interacting with methanol (MeOH), and 7-Hydroxyquinoline (HQ) interacting with H₂O. The uncoupled polarizability neglects the perturbation of the frozen system due to the external perturbation, whereas the coupled response includes the response of the environment and thus can be compared directly with supermolecular calculations. Within the FDE-pol method the coupled response is obtained by including local field effects. We show that FDE-pol can accurately reproduce both the exact uncoupled polarizability as well as the coupled polarizabilities of the supermolecular systems once local field effects are included. Using damped response theory we also demonstrate that the coupled frequency-dependent polarizability can be described by including local field effects. Our results show the necessity of including local field effects for describing the response properties of coupled subsystems, as well as the importance of accurate atomic polarizability models.

Acknowledgement

L.J. acknowledges support from the DE-SC0018038 awards. Portions of this work were conducted with Advanced CyberInfrastructure computational resources provided by The Institute for CyberScience at The Pennsylvania State University (<http://ics.psu.edu>).

Supplementary Information

The supplementary information contains the method to calculate the Hirshfeld polarizabilities, percent errors with respect to the DFT data for the polarizability components for each fragment from different methods, variation of polarizabilities with respect to DFT data for different functionals and basis sets before and after scaling, atomic polarizability parameters for atoms in each fragment, the plot of global parametric fit against the reference database, and comparison of Hirshfeld polarizability components to the global set and the DFT data.

References

- (1) Huang, C.; Pavone, M.; Carter, E. A. Quantum mechanical embedding theory based on a unique embedding potential. *J. Chem. Phys.* **2011**, *134*, 154110.
- (2) Nãbo, L. J.; Olsen, J. M. H.; Martínez, T. J.; Kongsted, J. The quality of the embedding potential is decisive for minimal quantum region size in embedding calculations: the case of the green fluorescent protein. *J. Chem. Theor. Comput.* **2017**, *13*, 6230–6236.
- (3) Neugebauer, J. Chromophore-Specific Theoretical Spectroscopy: From Subsystem Density Functional Theory to Mode-Specific Vibrational Spectroscopy. *Phys. Rev.* **2010**, *489*, 1–87.
- (4) Scholz, L.; Tölle, J.; Neugebauer, J. Analysis of environment response effects on excitation energies within subsystem-based time-dependent density-functional theory. *Int. J. Quantum Chem.* **2020**, *120*, e26213.
- (5) Knizia, G.; Chan, G. K.-L. Density matrix embedding: A simple alternative to dynamical mean-field theory. *Phys. Rev. Lett.* **2012**, *109*, 186404.
- (6) Sun, Q.; Chan, G. K.-L. Quantum embedding theories. *Acc. Chem. Res.* **2016**, *49*, 2705–2712.
- (7) Manby, F. R.; Stella, M.; Goodpaster, J. D.; Miller, T. F. A Simple, Exact Density-Functional-Theory Embedding Scheme. *J. Chem. Theor. Comput.* **2012**, *8*, 2564–2568.
- (8) Gomes, A. S. P.; Jacob, C. R. Quantum-chemical embedding methods for treating local electronic excitations in complex chemical systems. *Annu. Rep. Prog. Chem., Sect. C: Phys. Chem.* **2012**, *108*, 222–277.
- (9) Schnieders, D.; Neugebauer, J. Accurate embedding through potential reconstruction: A comparison of different strategies. *J. Chem. Phys.* **2018**, *149*, 054103.

- (10) Gordon, M. S.; Fedorov, D. G.; Pruitt, S. R.; Slipchenko, L. V. Fragmentation Methods: A Route to Accurate Calculations on Large Systems. *Chem. Rev.* **2012**, *112*, 632–672.
- (11) Raghavachari, K.; Saha, A. Accurate composite and fragment-based quantum chemical models for large molecules. *Chem. Rev.* **2015**, *115*, 5643–5677.
- (12) Senatore, G.; Subbaswamy, K. R. Density Dependence of the Dielectric Constant of Rare-Gas Crystals. *Phys. Rev. B* **1986**, *34*, 5754–5757.
- (13) Cortona, P. Self-consistently determined properties of solids without band-structure calculations. *Phys. Rev. B* **1991**, *44*, 8454–8458.
- (14) Fedorov, D. G.; Kitaura, K. Extending the power of quantum chemistry to large systems with the fragment molecular orbital method. *J. Phys. Chem. A* **2007**, *111*, 6904–6914.
- (15) Gordon, M. S.; Fedorov, D. G.; Pruitt, S. R.; Slipchenko, L. V. Fragmentation methods: A route to accurate calculations on large systems. *Chem. Rev.* **2012**, *112*, 632–672.
- (16) Laricchia, S.; Fabiano, E.; Sala, F. D. Semilocal and hybrid density embedding calculations of ground-state charge-transfer complexes. *J. Chem. Phys.* **2013**, *138*, 124112.
- (17) van Leeuwen, R.; Baerends, E. J. Exchange-correlation potential with correct asymptotic behavior. *Phys. Rev. A* **1994**, *49*, 2421.
- (18) Wu, Q.; Yang, W. A direct optimization method for calculating density functionals and exchange–correlation potentials from electron densities. *J. Chem. Phys.* **2003**, *118*, 2498–2509.
- (19) Zhang, X.; Carter, E. A. Kohn-Sham potentials from electron densities using a matrix representation within finite atomic orbital basis sets. *J. Chem. Phys.* **2018**, *148*, 034105.

- (20) Goodpaster, J. D.; Barnes, T. A.; Manby, F. R.; Miller, T. F. Accurate and systematically improvable density functional theory embedding for correlated wavefunctions. *J. Chem. Phys.* **2014**, *140*, 18A507.
- (21) Stoll, H.; Paulus, B.; Fulde, P. On the Accuracy of Correlation-Energy Expansions in Terms of Local Increments. *J. Chem. Phys.* **2005**, *123*, 144108.
- (22) Mata, R. A.; Werner, H.-J.; Schütz, M. Correlation Regions Within a Localized Molecular Orbital Approach. *J. Chem. Phys.* **2008**, *128*, 144106.
- (23) Henderson, T. M. Embedding Wave Function Theory in Density Functional Theory. *J. Chem. Phys.* **2006**, *125*, 014105.
- (24) Chulhai, D. V.; Jensen, L. Frozen Density Embedding with External Orthogonality in Delocalized Covalent Systems. *J. Chem. Theor. Comput.* **2015**, *11*, 3080–3088.
- (25) Jacob, C. R.; Neugebauer, J. Subsystem Density-Functional Theory. *Wiley Interdiscip. Rev.: Comput. Mol. Sci.* **2014**, *4*, 325–362.
- (26) Wesolowski, T. A.; Shedge, S.; Zhou, X. Frozen-density embedding strategy for multilevel simulations of electronic structure. *Chem. Rev.* **2015**, *115*, 5891–5928.
- (27) Götz, A. W.; Beyhan, S. M.; Visscher, L. Performance of Kinetic Energy Functionals for Interaction Energies in a Subsystem Formulation of Density Functional Theory. *J. Chem. Theor. Comput.* **2009**, *5*, 3161–3174.
- (28) Banafsheh, M.; Adam Wesolowski, T. Nonadditive kinetic potentials from inverted Kohn–Sham problem. *Int. J. Quantum Chem.* **2018**, *118*, e25410.
- (29) Pal, P. P.; Liu, P.; Jensen, L. Polarizable Frozen Density Embedding with External Orthogonalization. *J. Chem. Theor. Comput.* **2019**, *15*, 6588–6596.
- (30) Warshel, A.; Levitt, M. Theoretical Studies of Enzymic Reactions: Dielectric, Electrostatic and Steric Stabilization of the Carbonium Ion in the Reaction of Lysozyme. *J. Mol. Biol.* **1976**, *103*, 227–249.

- (31) Thole, B. T.; van Duijnen, P. T. On the quantum mechanical treatment of solvent effects. *Theor. Chim. Acta* **1980**, *55*, 307–318.
- (32) Singh, U. C.; Kollman, P. A. A combined ab initio quantum mechanical and molecular mechanical method for carrying out simulations on complex molecular systems: Applications to the CH₃Cl+ Cl⁻ exchange reaction and gas phase protonation of polyethers. *J. Comput. Chem.* **1986**, *7*, 718–730.
- (33) Bash, P. A.; Field, M. J.; Karplus, M. Free energy perturbation method for chemical reactions in the condensed phase: a dynamic approach based on a combined quantum and molecular mechanics potential. *J. Am. Chem. Soc.* **1987**, *109*, 8092–8094.
- (34) Field, M. J.; Bash, P. A.; Karplus, M. A combined quantum mechanical and molecular mechanical potential for molecular dynamics simulations. *J. Comput. Chem.* **1990**, *11*, 700–733.
- (35) Luzhkov, V.; Warshel, A. Microscopic models for quantum mechanical calculations of chemical processes in solutions: LD/AMPAC and SCAAS/AMPAC calculations of solvation energies. *J. Comput. Chem.* **1992**, *13*, 199–213.
- (36) Stanton, R. V.; Hartsough, D. S.; Merz Jr, K. M. Calculation of solvation free energies using a density functional/molecular dynamics coupled potential. *J. Phys. Chem. A* **1993**, *97*, 11868–11870.
- (37) De Vries, A.; Van Duijnen, P. T.; Juffer, A.; Rullmann, J.; Dijkman, J.; Merenga, H.; Thole, B. T. Implementation of reaction field methods in quantum chemistry computer codes. *J. Comput. Chem.* **1995**, *16*, 37–55.
- (38) Tuñón, I.; Martins-Costa, M. T.; Millot, C.; Ruiz-López, M. F.; Rivail, J.-L. A coupled density functional-molecular mechanics Monte Carlo simulation method: The water molecule in liquid water. *J. Comput. Chem.* **1996**, *17*, 19–29.

- (39) Gao, J. Methods and applications of combined quantum mechanical and molecular mechanical potentials. *Rev. Comput. Chem.* **1996**, *7*, 119–186.
- (40) Gao, J. Hybrid quantum and molecular mechanical simulations: an alternative avenue to solvent effects in organic chemistry. *Acc. Chem. Res.* **1996**, *29*, 298–305.
- (41) Lin, H.; Truhlar, D. G. QM/MM: what have we learned, where are we, and where do we go from here? *J. Mol. Struct.: THEOCHEM* **2007**, *117*, 185.
- (42) Thompson, M. A. QM/MMpol: A consistent model for solute/solvent polarization. Application to the aqueous solvation and spectroscopy of formaldehyde, acetaldehyde, and acetone. *J. Phys. Chem.* **1996**, *100*, 14492–14507.
- (43) Jensen, L.; van Duijnen, P. T.; Snijders, J. G. A discrete solvent reaction field model within density functional theory. *J. Chem. Phys.* **2003**, *118*, 514–521.
- (44) Olsen, J. M.; Aidas, K.; Kongsted, J. Excited states in solution through polarizable embedding. *J. Chem. Theor. Comput.* **2010**, *6*, 3721–3734.
- (45) Pedersen, M. N.; Hedegård, E. D.; Olsen, J. M. H.; Kauczor, J.; Norman, P.; Kongsted, J. Damped response theory in combination with polarizable environments: The polarizable embedding complex polarization propagator method. *J. Chem. Theor. Comput.* **2014**, *10*, 1164–1171.
- (46) List, N. H.; Olsen, J. M. H.; Kongsted, J. Excited states in large molecular systems through polarizable embedding. *Phys. Chem. Chem. Phys.* **2016**, *18*, 20234–20250.
- (47) List, N. H.; Jensen, H. J. A.; Kongsted, J. Local electric fields and molecular properties in heterogeneous environments through polarizable embedding. *Phys. Chem. Chem. Phys.* **2016**, *18*, 10070–10080.
- (48) Day, P. N.; Jensen, J. H.; Gordon, M. S.; Webb, S. P.; Stevens, W. J.; Krauss, M.; Garmer, D.; Basch, H.; Cohen, D. An effective fragment method for modeling

- solvent effects in quantum mechanical calculations. *J. Chem. Phys.* **1996**, *105*, 1968–1986.
- (49) Sneskov, K.; Schwabe, T.; Christiansen, O.; Kongsted, J. Scrutinizing the effects of polarization in QM/MM excited state calculations. *Phys. Chem. Chem. Phys.* **2011**, *13*, 18551–18560.
- (50) Mennucci, B. Modeling environment effects on spectroscopies through QM/classical models. *Phys. Chem. Chem. Phys.* **2013**, *15*, 6583–6594.
- (51) Bondanza, M.; Nottoli, M.; Cupellini, L.; Lipparini, F.; Mennucci, B. Polarizable embedding QM/MM: the future gold standard for complex (bio) systems? *Phys. Chem. Chem. Phys.* **2020**, *22*, 14433–14448.
- (52) Schröder, H.; Schwabe, T. Efficient determination of accurate atomic polarizabilities for polarizable embedding calculations. *J. Comput. Chem.* **2016**, *37*, 2052–2059.
- (53) Reinholdt, P.; Kongsted, J.; Olsen, J. M. H. Polarizable Density Embedding: A Solution to the Electron Spill-Out Problem in Multiscale Modeling. *J. Phys. Chem. Lett.* **2017**, *8*, 5949–5958, PMID: 29178794.
- (54) Olsen, J. M. H.; Steinmann, C.; Ruud, K.; Kongsted, J. Polarizable Density Embedding: A New QM/QM/MM-Based Computational Strategy. *J. Phys. Chem. A* **2015**, *119*, 5344–5355.
- (55) List, N. H.; Norman, P.; Kongsted, J.; Jensen, H. J. A. A quantum-mechanical perspective on linear response theory within polarizable embedding. *J. Chem. Phys.* **2017**, *146*, 234101.
- (56) Chulhai, D. V.; Jensen, L. External orthogonality in subsystem time-dependent density functional theory. *Phys. Chem. Chem. Phys.* **2016**, *18*, 21032–21039.

- (57) Höfener, S.; Gomes, A. S. P.; Visscher, L. Solvatochromic shifts from coupled-cluster theory embedded in density functional theory. *J. Chem. Phys.* **2013**, *139*, 104106.
- (58) Rinaldi, J. M.; Morton, S. M.; Jensen, L. A Discrete Interaction Model/Quantum Mechanical Method for Simulating Nonlinear Optical Properties of Molecules near Metal Surfaces. *Mol. Phys.* **2013**, *111*, 1322–1331.
- (59) Casida, M. E.; Wesolowski, T. A. Generalization of the Kohn-Sham Equations with Constrained Electron Density Formalism and its Time-Dependent Response Theory Formulation. *Int. J. Quantum Chem.* **2004**, *96*, 577–588.
- (60) Neugebauer, J. Couplings between electronic transitions in a subsystem formulation of time-dependent density functional theory. *J. Chem. Phys.* **2007**, *126*, 134116.
- (61) Reis, H.; Papadopoulos, M. G.; Hättig, C.; Ángyán, J. G.; Munn, R. W. Distributed first and second order hyperpolarizabilities: An improved calculation of nonlinear optical susceptibilities of molecular crystals. *J. Chem. Phys.* **2000**, *112*, 6161–6172.
- (62) Jensen, L.; Swart, M.; van Duijnen, P. T. Microscopic and macroscopic polarization within a combined quantum mechanics and molecular mechanics model. *J. Chem. Phys.* **2005**, *122*, 034103.
- (63) Wortmann, R.; Bishop, D. M. Effective polarizabilities and local field corrections for nonlinear optical experiments in condensed media. *J. Chem. Phys.* **1998**, *108*, 1001–1007.
- (64) Cammi, R.; Mennucci, B.; Tomasi, J. An attempt to bridge the gap between computation and experiment for nonlinear optical properties: macroscopic susceptibilities in solution. *J. Phys. Chem. A* **2000**, *104*, 4690–4698.

- (65) Jensen, L.; Åstrand, P.-O.; Mikkelsen, K. V. Microscopic and Macroscopic Polarization in C60 Fullerene Clusters as Calculated by an Electrostatic Interaction Model. *J. Phys. Chem. B* **2004**, *108*, 8226–8233.
- (66) Payton, J. L.; Morton, S. M.; Moore, J. E.; Jensen, L. A Hybrid Atomistic Electrodynamics–Quantum Mechanical Approach for Simulating Surface-Enhanced Raman Scattering. *Acc. Chem. Res.* **2014**, *47*, 88–99.
- (67) Chulhai, D. V.; Jensen, L. Simulating Surface-Enhanced Raman Optical Activity Using Atomistic Electrodynamics-Quantum Mechanical Models. *J. Phys. Chem. A* **2014**, *118*, 9069–9079.
- (68) Chulhai, D. V.; Jensen, L. Plasmonic Circular Dichroism of 310- and α -Helix Using a Discrete Interaction Model/Quantum Mechanics Method. *J. Phys. Chem. A* **2015**, *119*, 5218–5223.
- (69) Hunt, K. L. C. Nonlocal polarizability densities and van der Waals interactions. *J. Chem. Phys.* **1983**, *78*, 6149–6155.
- (70) Hunt, K. L. C. Nonlocal polarizability densities and the effects of short-range interactions on molecular dipoles, quadrupoles, and polarizabilities. *J. Chem. Phys.* **1984**, *80*, 393–407.
- (71) Jensen, L. L.; Jensen, L. Electrostatic Interaction Model for the Calculation of the Polarizability of Large Noble Metal Nanoclusters. *J. Phys. Chem. C* **2008**, *112*, 15697–15703.
- (72) Tkatchenko, A.; Scheffler, M. Accurate Molecular Van Der Waals Interactions from Ground-State Electron Density and Free-Atom Reference Data. *Phys. Rev. Lett.* **2009**, *102*, 073005.
- (73) Schwerdtfeger, P.; Nagle, J. K. 2018 Table of static dipole polarizabilities of the neutral elements in the periodic table. *Mol. Phys.* **2019**, *117*, 1200–1225.

- (74) Tkatchenko, A.; DiStasio, R. A.; Car, R.; Scheffler, M. Accurate and Efficient Method for Many-Body van der Waals Interactions. *Phys. Rev. Lett.* **2012**, *108*, 236402.
- (75) Mayer, A. Formulation in terms of normalized propagators of a charge-dipole model enabling the calculation of the polarization properties of fullerenes and carbon nanotubes. *Phys. Rev. B* **2007**, *75*, 045407.
- (76) Elking, D.; Darden, T.; Woods, R. J. Gaussian induced dipole polarization model. *J. Comput. Chem.* **2007**, *28*, 1261–1274.
- (77) Jensen, L. L.; Jensen, L. Atomistic Electrodynamics Model for Optical Properties of Silver Nanoclusters. *J. Phys. Chem. C* **2009**, *113*, 15182–15190.
- (78) Morton, S. M.; Jensen, L. A Discrete Interaction Model/Quantum Mechanical Method for Describing Response Properties of Molecules Adsorbed on Metal Nanoparticles. *J. Chem. Phys.* **2010**, *133*, 074103.
- (79) Gritsenko, O.; Schipper, P.; Baerends, E. Approximation of the exchange-correlation Kohn-Sham potential with a statistical average of different orbital model potentials. *Chem. Phys. Lett.* **1999**, *302*, 199 – 207.
- (80) Sasagane, K.; Aiga, F.; Itoh, R. Higher-order response theory based on the quasienergy derivatives: The derivation of the frequency-dependent polarizabilities and hyperpolarizabilities. *J. Chem. Phys.* **1993**, *99*, 3738–3778.
- (81) Christiansen, O.; Jørgensen, P.; Hättig, C. Response functions from Fourier component variational perturbation theory applied to a time-averaged quasienergy. *Int. J. Quantum Chem.* **1998**, *68*, 1.
- (82) Boyd, R. W. *Nonlinear Optics*; Academic Press: San Diego, 1992.
- (83) Jensen, L.; Autschbach, J.; Schatz, G. C. Finite Lifetime Effects on the Polarizability Within Time-Dependent Density-Functional Theory. *J. Chem. Phys.* **2005**, *122*, 224115.

- (84) Hu, Z.; Autschbach, J.; Jensen, L. Simulation of resonance hyper-Rayleigh scattering of molecules and metal clusters using a time-dependent density functional theory approach. *J. Chem. Phys.* **2014**, *141*, 124305.
- (85) Krykunov, M.; Autschbach, J. Calculation of optical rotation with time-periodic magnetic-field-dependent basis functions in approximate time-dependent density-functional theory. *J. Chem. Phys.* **2005**, *123*, 114103.
- (86) Karna, S. P.; Dupuis, M. Frequency dependent nonlinear optical properties of molecules: Formulation and implementation in the HONDO program. *J. Comput. Chem.* **1991**, *12*, 487–504.
- (87) van Gisbergen, S. J. A.; Snijders, J. G.; Baerends, E. J. Calculating frequency-dependent hyperpolarizabilities using time-dependent density functional theory. *J. Chem. Phys.* **1998**, *109*, 10644–10656.
- (88) Hu, Z.; Autschbach, J.; Jensen, L. Simulating Third-Order Nonlinear Optical Properties Using Damped Cubic Response Theory within Time-Dependent Density Functional Theory. *J. Chem. Theor. Comput.* **2016**, *12*, 1294–1304.
- (89) Baerends, E.; Autschbach, J.; Bérces, A.; Bickelhaupt, F.; Bo, C.; Boerrigter, P.; Cavallo, L.; Chong, D.; Deng, L.; Dickson, R.; Ellis, D.; van Faassen, M.; Fan, L.; Fischer, T.; Guerra, C. F.; van Gisbergen, S.; Götz, A.; Groeneveld, J.; Gritsenko, O.; Grüning, M.; Harris, F.; van den Hoek, P.; Jacob, C.; Jacobsen, H.; Jensen, L.; van Kessel, G.; Kootstra, F.; Krykunov, M.; van Lenthe, E.; McCormack, D.; Michalak, A.; Neugebauer, J.; Nicu, V.; Osinga, V.; Patchkovskii, S.; Philippsen, P.; Post, D.; Pye, C.; Ravenek, W.; Rodriguez, J.; Ros, P.; Schipper, P.; Schreckenbach, G.; Snijders, J.; Solà, M.; Swart, M.; Swerhone, D.; te Velde, G.; Vernooijs, P.; Versluis, L.; Visscher, L.; Visser, O.; Wang, F.; Wesolowski, T.; van Wezenbeek, E.; Wiesenekker, G.; Wolff, S.; Woo, T.; Yakovlev, A.; Ziegler, T. Amsterdam Density Functional. 2008; <http://www.scm.com>.

- (90) Wilkins, D. M.; Grisafi, A.; Yang, Y.; Lao, K. U.; DiStasio, R. A.; Ceriotti, M. Accurate molecular polarizabilities with coupled cluster theory and machine learning. *Proc. Natl. Acad. Sci. USA* **2019**, *116*, 3401–3406.
- (91) Neugebauer, J. On the calculation of general response properties in subsystem density functional theory. *J. Chem. Phys.* **2009**, *131*, 084104.
- (92) Artiukhin, D. G.; Jacob, C. R.; Neugebauer, J. Excitation energies from frozen-density embedding with accurate embedding potentials. *J. Chem. Phys.* **2015**, *142*, 234101.
- (93) Perdew, J. P.; Chevary, J. A.; Vosko, S. H.; Jackson, K. A.; Pederson, M. R.; Singh, D. J.; Fiolhais, C. Atoms, molecules, solids, and surfaces: Applications of the generalized gradient approximation for exchange and correlation. *Phys. Rev. B* **1992**, *46*, 6671–6687.
- (94) Perdew, J. P.; Burke, K.; Ernzerhof, M. Generalized Gradient Approximation Made Simple. *Phys. Rev. Lett.* **1996**, *77*, 3865–3868.

Graphical TOC Entry

